PAPER

Electronic and optical properties of $B_xC_yN_z$ hybrid α-graphynes†

A. Freitas, [ID] *[a] L. D. Machado, [ID] [a] C. G. Bezerra, [ID] [a] R. M. Tromer[a] and S. Azevedo [ID] [b]

Hybrid two-dimensional (2D) materials composed of carbon, boron, and nitrogen constitute a hot topic of research, as their flexible composition allows for tunable properties. However, while graphene-like hybrid lattices have been well characterized, systematic investigations are lacking for various 2D materials. Hence, in the present contribution, we employ first-principles calculations to investigate the structural, electronic and optical properties of what we call $B_xC_yN_z$ hybrid α-graphynes. We considered eleven structures with stoichiometry BC_2N and varied atomic arrangements. We calculated the formation energy for each arrangement, and determined that it is low (high) when the number of boron-carbon and nitrogen-carbon bonds is low (high). We found that the formation energy of many our structures compared favorably with a previous literature proposal. Regarding the electronic properties, we found that the investigated structures are semiconducting, with band gaps ranging from 0.02 to 2.00 eV. Moreover, we determined that most of the $B_xC_yN_z$ hybrid α-graphynes proposed here strongly absorb infrared light, and so could potentially find applications in optoelectronic devices such as heat sensors and infrared filters.

I. Introduction

In the last decade, two-dimensional (2D) nanoscale materials have attracted considerable interest due to their innovative physical properties and potential applications in many emerging technologies. Examples of 2D materials which have already been synthesized and extensively studied include graphene[1,2] and hexagonal boron nitride (h-BN).[3,4] Both structures are composed of sp^2-hybridized atoms arranged in a honeycomb lattice. Graphene is a zero-band-gap semiconductor, which presents high electron mobility, high thermal conductivity, high strength, and flexibility.[5-8] On the other hand, h-BN is a wide-gap semiconductor (>4 eV), with mechanical properties similar to graphene, and high resistance to oxidation and degradation.[9-11] In this context, it is worth pointing out that the substitution of C atoms in graphene by B and N atoms leads to the formation of $B_xC_yN_z$ hexagonal hybrid sheets,[12-14] which have also been extensively investigated and have recently been synthesized.[15,16] They present a variety of energy gaps (<2 eV) that are intermediate between those found in graphene and h-BN. Moreover, these materials can exhibit either metallic or semiconducting behavior, depending on the atomic arrangement of C, B, and N atoms.[17-21] Hence, $B_xC_yN_z$ hexagonal sheets

are promising materials for the manufacture of nanoscale electronic devices.

Following the advent of two-dimensional honeycomb lattices, in recent years intense research has rapidly expanded the family of 2D materials. New structures include graphyne,[22,23] graphenylene,[24] phagraphene,[25] T-graphene[26] and others.[27] These materials have been theoretically proposed and some have already been synthesized. First-principles calculations predict interesting mechanical, optical, and electronic properties for these structures, making them promising candidates for future technological applications. Among the cited examples, the group of materials called "graphynes" has attracted much attention.

Graphynes are 2D structures composed of a mixture of sp and sp^2-hybridized carbon atoms. This is in contrast to graphene, where all carbon atoms are sp^2-hybridized. Graphynes were initially predicted by Baughman *et al.*[28] and it has since received considerable attention. Theoretically, these structures are formed by the combination of carbon hexagons with polyyne-like carbon linear chains (…–C≡C–C≡C–…).[29] Although graphyne sheets have not yet been synthesized, small graphyne flakes have already been successfully obtained.[30-33] In addition, large area films of graphdiyne, a related material, were produce on a copper substrate *via* a cross-coupling reaction by Li *et al.*[34] The sp and sp^2 carbon atoms can be combined in various ways, and so far four graphyne types have been investigated, namely α-, β-, γ-, and 6, 6, 12-. The α-, β-, and 6, 6, 12-graphynes are metallic, and all feature Dirac cones in their electronic band structure;[35,36] meanwhile, γ-graphyne is a semiconductor.[37] All four of them have been proposed as suitable materials for applications in nanoelectronics.

[a]Departamento de Física, Universidade Federal do Rio Grande do Norte, 59072-970, Natal, RN, Brazil. E-mail: alilianefisica@yahoo.com.br

[b]Departamento de Física, CCEN, Universidade Federal da Paraíba, Caixa Postal 5008, 58051-970, João Pessoa, PB, Brazil
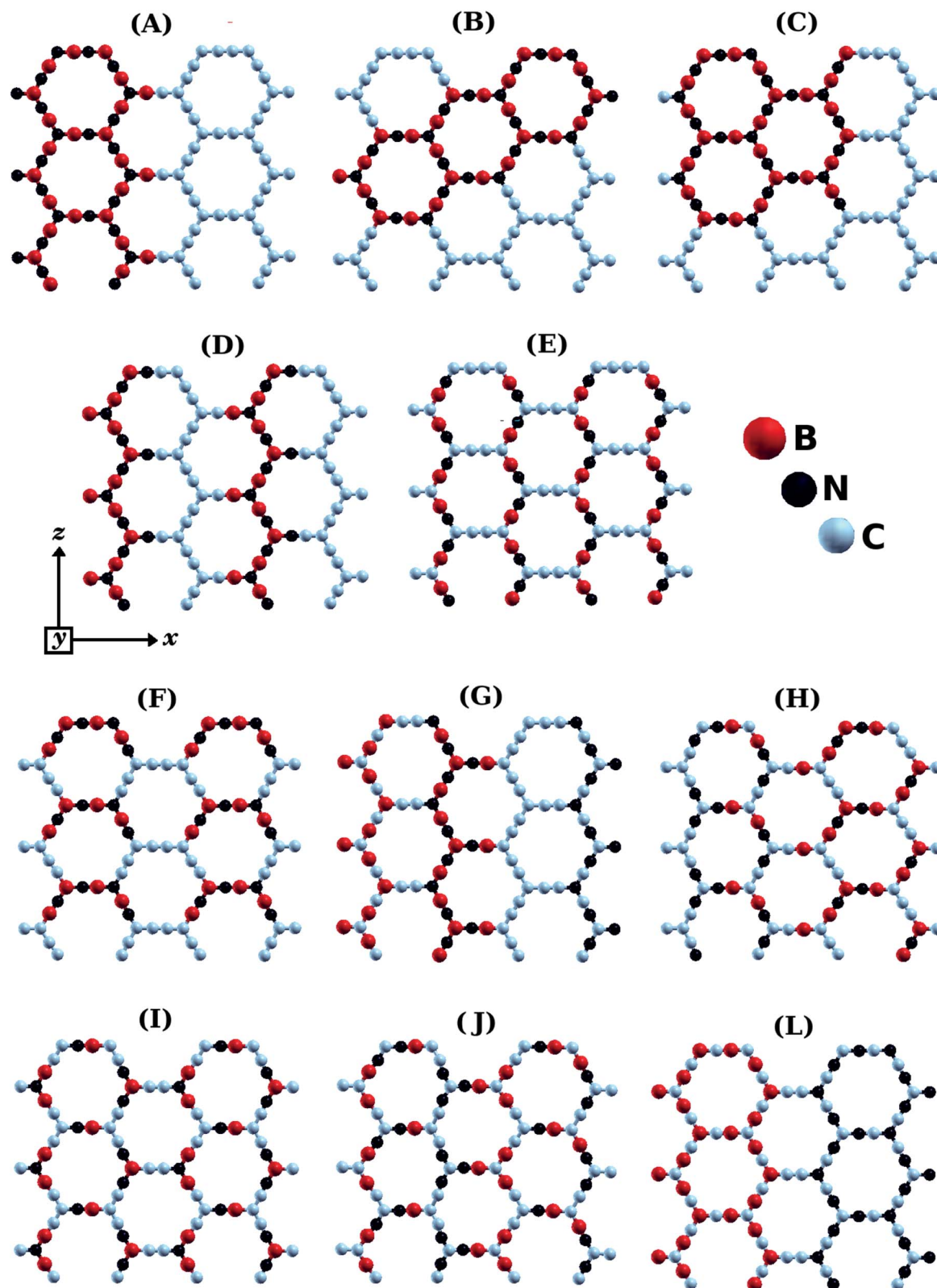
† PACS numbers: 73.20.At, 73.20.Hb, 71.15.Mb.

Fig. 1 Illustration of the optimized $B_xC_yN_z$ hybrid α-graphynes with different atomic arrangements.

Additional applications proposed for graphynes include: energy storage,[38] use as battery anodes,[39] gas separation,[40] and water desalination.[41] Boron nitride analogues of the α-, β-, γ-, and 6, 6, 12- graphynes have also been investigated.[42–44] These structures, termed BNynes, are formed by the combination of BN hexagonal rings with BN linear chains (…−B≡N−B≡N−…). First-

principles calculations, performed by Zhang *et al.*[45] and Cao *et al.*,[46] have shown that BNynes are wide-gap semiconductors (>4 eV), with strong absorption in a wide UV photon-energy region.

Among the investigated graphynes and BNynes, α-graphyne and α-BNyne have received considerable attention.[47–50] To obtain α-graphyne, carbon linear chains (containing n atoms) are inserted in each C–C bond of graphene, leading to a honeycomb-like lattice with large hexagonal rings. Corner atoms are tri-coordinated in each hexagon, as in graphene. Similarly, α-BNyne is obtained by the insertion of BN linear chains in each B–N bond of h-BN. Ongun *et al.* have carried out *ab initio* calculations to test the structural stability and to determine the electronic and mechanical properties of α-graphyne and α-BNyne, as a function of the number of atoms n contained in the linear chains.[51] The authors calculated the phonon modes and performed finite-temperature molecular dynamics, and determined that both α-graphyne and α-BNyne are stable for even values of n and unstable for odd values of n. High stability was found for $n = 2$. Regarding the electronic properties, they found that all α-graphynes are metallic, while all α-BNynes are wide-gap semiconductors.

An interesting possibility regarding α-graphyne and α-BNyne would be to combine the properties of these materials through the formation of $B_xC_yN_z$ hybrid sheets, in the same way as done for graphene and h-BN.[12–14,17–21] Recently, the electronic structure and the structural stability of α-graphynes, doped with different concentrations of BN pairs, was investigated *via* first-principles calculations by Yun *et al.*[52] and Deng *et al.*[53] Both authors observed the opening of an energy-gap in the electronic spectrum of α-graphyne, for any BN pair concentration. Additionally, it was determined that the band gap was proportional to the dopant concentration. Thus, α-graphynes doped with BN pairs are semiconductors with tunable band gap. On the other hand, to our knowledge, there are presently no studies in the literature investigating island- and stripe-like atomic arrangements of B, C, and N atoms in α-graphyne sheets. Such atomic arrangements minimize formation energy and maximize stability in $B_xC_yN_z$ hybrid graphenes.[12] With this motivation in mind, and also considering the growing interest in $B_xC_yN_z$ hybrid nanostructures, in this paper we perform first-principles calculations to investigate the stability, as well as the electronic and optical properties, of what we call $B_xC_yN_z$ hybrid α-graphynes.

II. Computational details and methods

Fig. 1 shows the $B_xC_yN_z$ hybrid α-graphynes investigated in this work. Similar to graphene, these structures are monolayers with hexagonal rings and three-coordinated atoms in each corner. We considered different atomic arrangements for an unit cell with 96 atoms. For comparison, unit cells for α-graphyne and α-BNyne contain only 8 atoms.[51] The large unit cells allow us to investigate island-like (Fig. 1B and C) and stripe-like (Fig. 1A and D–G) atomic arrangements, as was

done by Azevedo *et al.* for $B_xC_yN_z$ hybrid graphenes.[12] In island-like arrangements, we have the presence of $(BN)_x$ and C_y units of different sizes and forms; meanwhile, in stripe-like arrangements, we have BN and C stripes connected along a specific direction. Thus, the $B_xC_yN_z$ hybrid α-graphynes have different numbers of B–N, C–C, B–C, and N–C bonds. The chosen atomic arrangements preclude the presence of energetically unfavorable B–B and N–N bonds.

The structures shown in Fig. 1 were then optimized using first-principles calculations based on density functional theory (DFT), as implemented in the SIESTA code.[54,55] We used the Generalized Gradient Approximation (GGA-PBE) for the exchange-correlation term.[56,57] A linear combination of numerical atomic orbitals was used to represent a double-ζ basis set with polarized functions (DZP). To modulate the strong interactions between electrons and core ions, we used the norm-conserving Troullier Martins pseudopotential[58] in the Kleinman–Bylander factorized form.[59] All calculations use a mesh cutoff of 150 Ry, with the Brillouin zone sampled by $3 \times 2 \times 2$ special k-points. It was adopted a convergence criterion where the self-consistency is achieved when the maximum difference between the output and the input of each element of the density matrix, in a self-consistent field cycle, is smaller than 10^{-4} eV. The optimization of atomic positions was allowed to proceed until the force on each atom was less than 0.1 eV Å^{-1}. We adopted a rectangular supercell and all calculations were performed at $T = 0$ K. The unit cell is repeated in the x and y directions, forming an infinite $B_xC_yN_z$ hybrid α-graphyne sheet. A large vacuum region of 20 Å was used along of the z direction, to avoid spurious interactions between two adjacent periodic images.
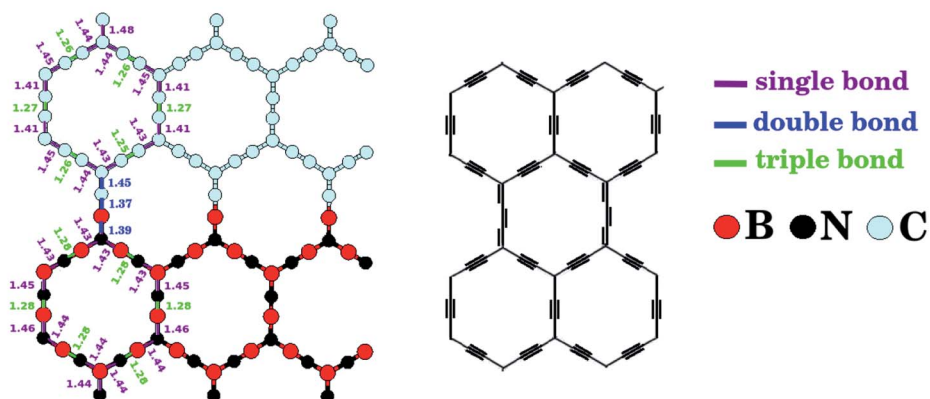
Note, however, that the DFT-LDA/GGA approach is known to underestimate band gaps,[60] and this can lead to incorrect predictions regarding the optical properties of a material. Several approaches have been developed to address this issue, including the so-called hybrid functionals and the GW approximation.[61–64] In particular, the hybrid functional HSE06 has been found to give a significantly improved description of

Table 1 Calculated formation energy (E_{Form}) for all investigated B_x-C_yN_z hybrid α-graphynes. R_b is the total number of 'regular' chemical bonds and W_b is the total number of 'wrong' chemical bonds. E_g is the energy band gap obtained with the PBE and HSE06 functionals
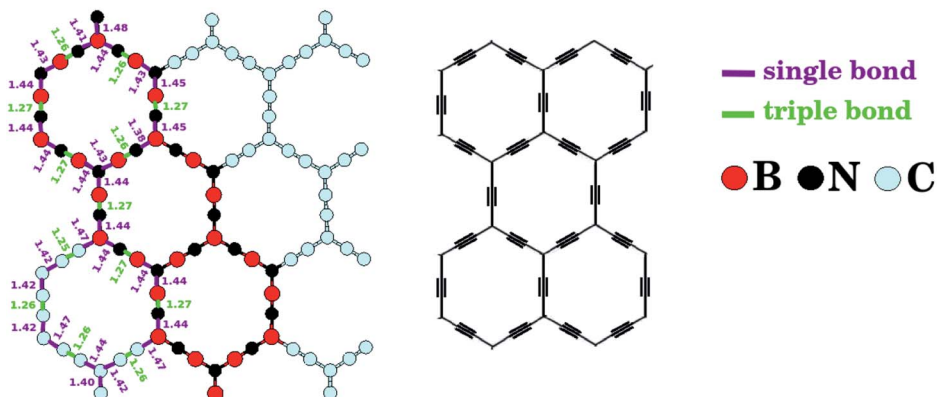
Structure	E_{form} (eV n_T^{-1})	R_b	W_b	R_b/W_b	E_g (GGA) (eV)	E_g (HSE06) (eV)
(A)	<u>0.06</u>	102	6	17	0.80	1.20
(B)	0.08	98	10	9.8	0.21	0.28
(C)	0.08	98	10	9.8	0.26	0.47
(D)	0.10	96	12	8.0	1.43	2.00
(E)	0.13	84	24	3.5	1.30	1.80
(F)	0.14	60	48	1.3	1.10	1.93
(G)	0.19	60	48	1.3	0.00	0.02
(H)	0.22	54	54	1.0	0.00	0.09
(I)	0.25	54	54	1.0	0.29	0.34
(J)	0.32	42	66	0.6	0.10	0.21
(L)	0.42	6	102	0.1	0.11	0.05

the electronic properties of nanomaterials.[65,66] Thus, for the $B_xC_yN_z$ hybrid α-graphynes investigated in this work, we also performed calculations of the electronic properties using the HSE06 functional, as implemented in the GAUSSIAN16 code.[67,68] A comparison between the results obtained with the GGA and HSE06 functionals is given below.

III. Results and discussion

In order to estimate the structural stability of the $B_xC_yN_z$ hybrid α-graphynes analyzed in the present study, we calculate the formation energy E_{Form} through a thermodynamic approach,

Fig. 2   Calculated bond length for the monolayers A, B, C and D shown in Fig. 1. The bond lengths illustrated repeat themselves periodically along the zigzag direction.
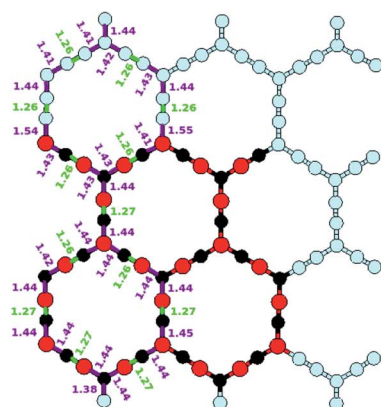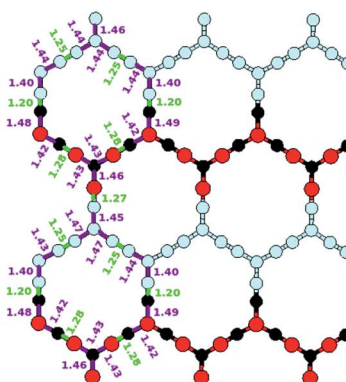
which is based on the prior determination of the chemical potentials of the atomic species involved in the synthesis reaction. The details of this approach are described in ref. 13 and 14. The formation energy is defined by the following expression

$$E_{\text{Form}} = \frac{E_{\text{T}} - n_{\text{B}}\mu_{\text{B}} - n_{\text{N}}\mu_{\text{N}} - n_{\text{C}}\mu_{\text{C}}}{n_{\text{atom}}}, \tag{1}$$

where E_{T} is the calculated total energy provided by the SIESTA code, n_{atom} is the total number of atoms in the structure, n_i (i = B, N, C) is the number of atoms for each element and μ_i is the corresponding chemical potential. Furthermore, the chemical potentials μ_{B}, μ_{N}, and μ_{C} satisfy the following conditions of thermodynamic equilibrium:

$$\mu_{\text{BN}} = \mu_{\text{B}} + \mu_{\text{N}} \text{ and } \mu_{\text{CC}} = \mu_{\text{C}} + \mu_{\text{C}}, \tag{2}$$

where the parameters μ_{BN} and μ_{CC} are the chemical potentials for the boron–nitrogen (BN) and carbon–carbon (CC) pairs, respectively. In this work, the chemical potentials for the CC and BN pairs were obtained by taking α-graphyne and α-BNyne
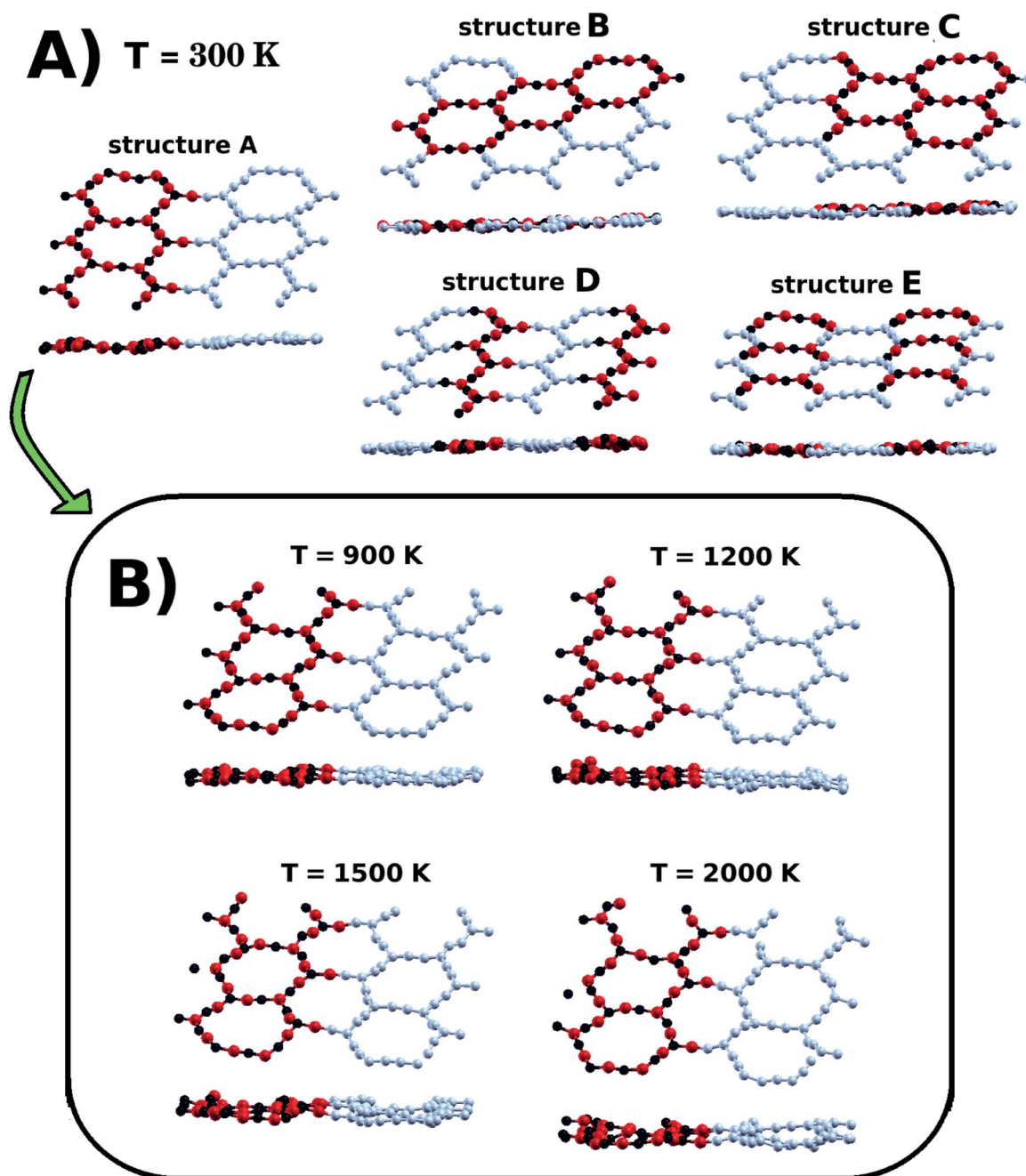

Fig. 3 In (A) we have snapshots from molecular dynamics simulations of the $B_xC_yN_z$ hybrid α-graphynes, after thermalization at $T = 300$ K. In (B) we have the snapshots of structure A after thermalization at various higher temperatures.

as references and assigning zero values to their formation energies. Thereby, through the use of eqn (1) and (2), we found that $\mu_{CC} = -307.58$ eV and $\mu_{BN} = -348.29$ eV. Lastly, for the $B_xC_yN_z$ hybrid α-graphynes studied in this work, we take into account that, in all cases, $n_B = n_N = n_{BN}$, and $n_{CC} = n_C/2$, so that the eqn (1) becomes

$$E_{Form} = (E_{Tot} - n_{BN}\mu_{BN} - n_{CC}\mu_{CC})/n_{atom}. \qquad (3)$$

The formation energies, obtained by using eqn (3), are quoted in the second column of Table 1. In this context, we observe that in each structure there is a relationship between E_{Form} and the number of "regular" chemical bonds, C–C and B–N, and "wrong" chemical bonds, C–B and C–N. Thus, in order to take into account this fact, we define the ratio R_b/W_b, where R_b and W_b denote the number of regular and wrong chemical bonds, respectively. This relationship has also been observed in other types of hybrid nanostructures with
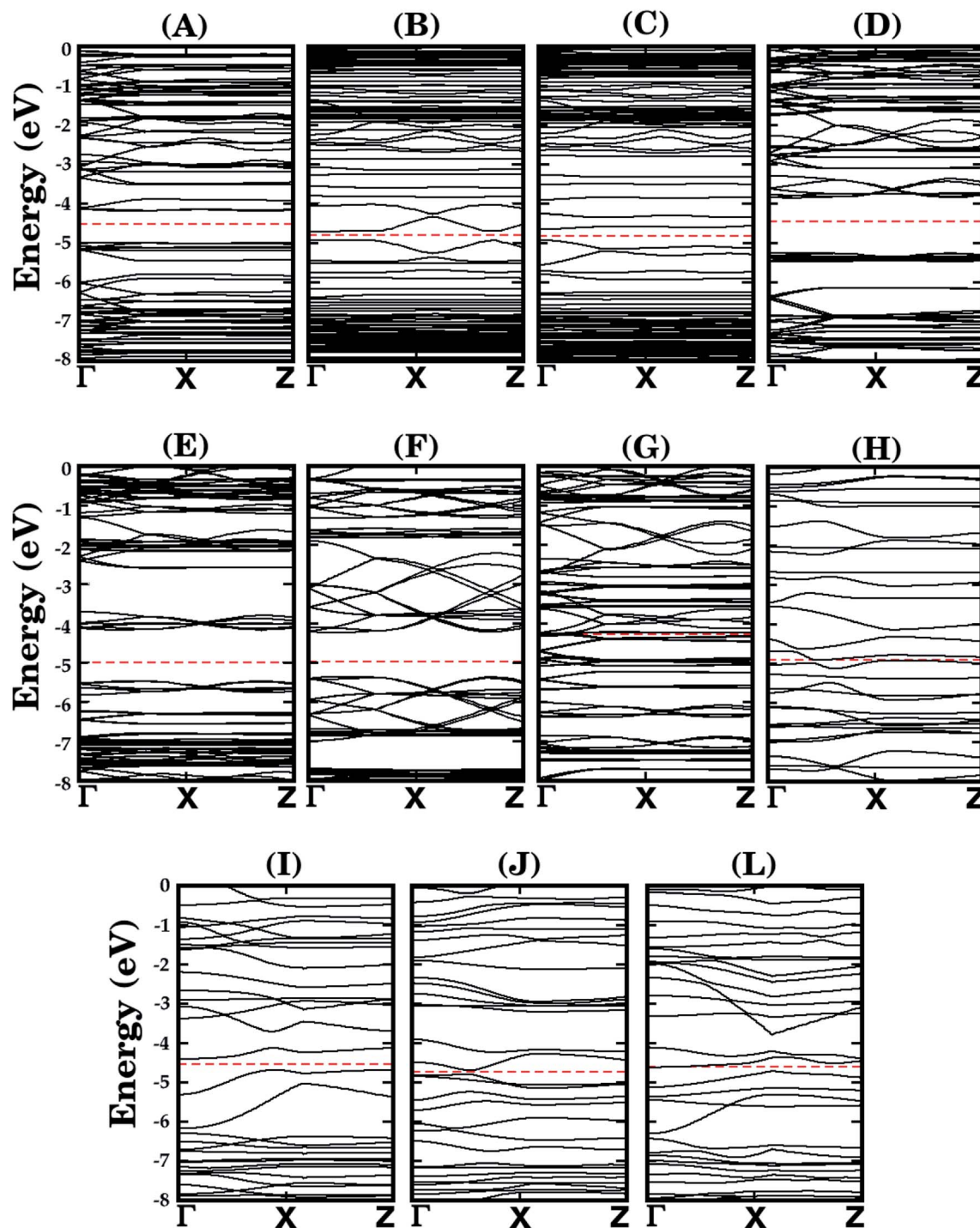

Fig. 4 Calculated band structures for the monolayers shown in Fig. 1. The dashed line represents the Fermi level.

$B_xC_yN_z$ stoichiometry.[17,18,69] The value of the ratio R_b/W_b, for each structure, is displayed in the fifth column of Table 1, where we notice that the formation energy increases as the number of regular bonds decreases, *i.e.*, when the ratio R_b/W_b decreases.

The lengths of the B–N, C–C, B–C, and N–C bonds in the relaxed $B_xC_yN_z$ hybrid α-graphynes are shown in Fig. 2. Since the hybridization state for a given B, C, or N atom can be either sp or sp^2, atoms of a given element are no longer chemically
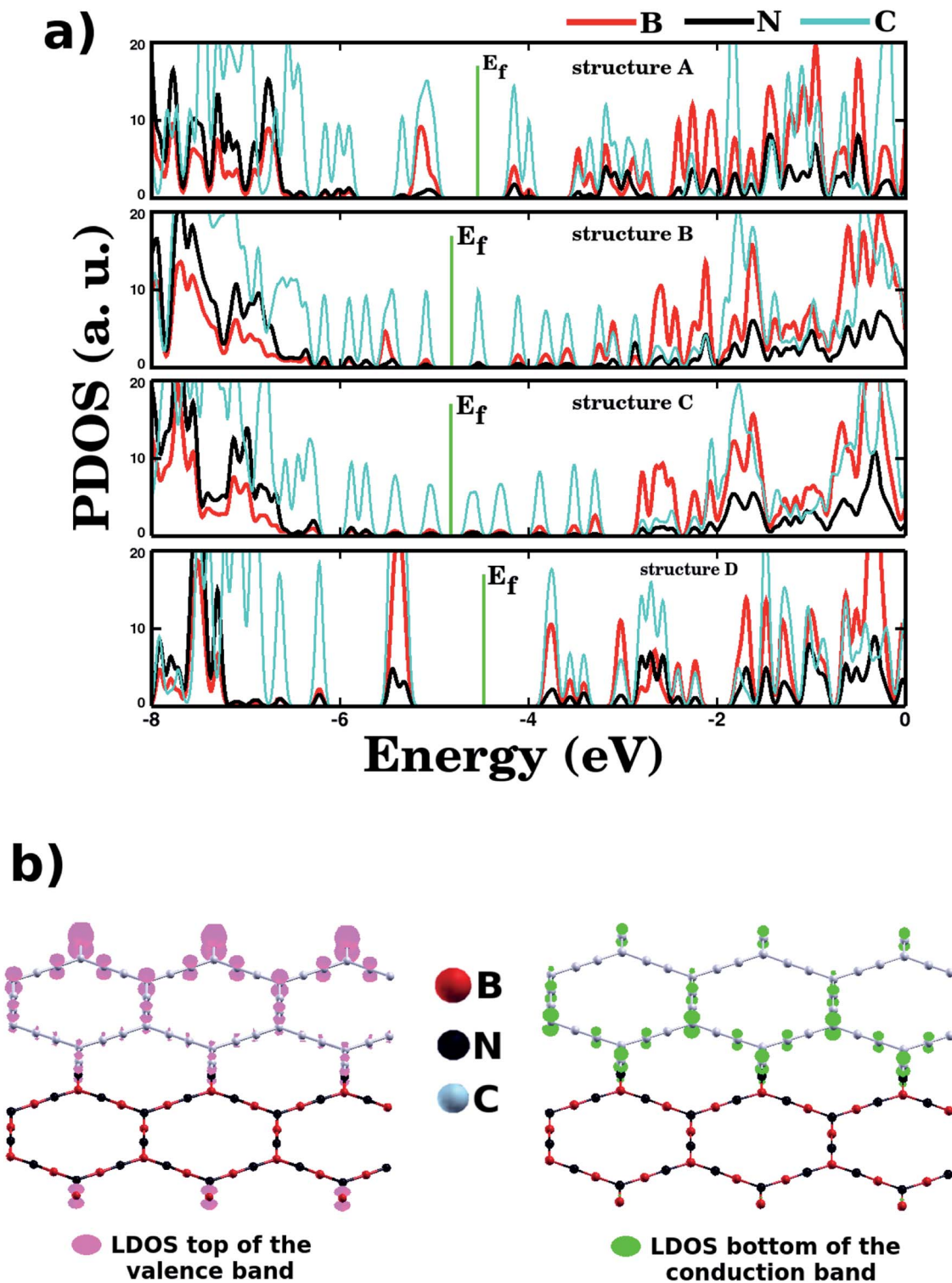

Fig. 5 (a) The calculated projected density of states (PDOS) of selected $B_xC_yN_z$ hybrid α-graphynes. The Fermi energy E_f is indicated by the dotted vertical line. (b) The local density of states (LDOS) associated with the bottom of the conduction band and the top of the valence band for the α-graphyne (A) structure.

equivalent, as they are in the cases of graphene[1] and h-BN.[11] Depending on the atomic arrangement of the sheet, we can have up to three different types of bonds: simple (X_{sp}–Y_{sp}^2), double (X_{sp}^2=Y_{sp}^2), and triple (X_{sp}≡Y_{sp}), where X and Y are variables that represent an B, C, or N atom. Structure A is the only that exhibits a lattice with the three types of bonds mentioned above. In this case, we observe a mixture of the following atomic chains: –C–C≡C–C–, –B–N≡B–N–, and –C=C=B=N– (see Fig. 2). The bonds in these chains are similar to those found in polyyne- or cumulene-type carbon linear chains. On the other hand, in all other structures, B, C, and N atoms are linked together through simple and triple bonds; that is, all atomic chains are of the type –X–Y≡Z–W– (X, Y, Z, and W are variables that represent B, C, and N atoms). Moreover, we find B–N and C–C bond lengths which are slightly smaller than those found for α-graphyne and α-BNyne in ref. 29 and 51. These subtle differences may be caused by different software performance or parameter setting.

From the data in Table 1, we can see that structure A, with the highest R_b/W_b ratio, presents the lowest value of E_{Form}, and so is the most stable structure. Following this line of reasoning, structures B and C, which exhibit the second lowest R_b/W_b ratio, are also the second most stable structures (the energy difference in comparison to structure A is only 0.02 eV/n_{at}). Structure A is stable due to its atomic arrangement, with stripes of BN and C hexagons connected in a way that minimizes the number of atoms in the interface between the two materials; this arrangement also introduces single, double, and triple bonds into the lattice (see Fig. 2). On the other hand, structures J and L, which have the highest values of E_{Form} (above 0.30 eV/n_{at}), are the most unstable. The common feature for these structures is the low R_b/W_b ratio, which, according to our results, is not a favorable trend for $B_xC_yN_z$ hybrid α-graphynes. We have also calculated the formation energy for a structure based on an α-graphyne motif that was investigated by Yun et al.[52] In particular, we examined the 2BN-αG monolayer,[52] which has B, N, and C concentrations equivalent to those found in our structures. By using eqn (3), we found a formation energy of 0.14 eV/n_{at} for 2BN-αG. By contrast, structure A has a formation energy of just 0.06 eV/n_{at}. This result is not surprising, as the R_b/W_b ratio for 2BN-αG is equal to 2, a rather low value.

We also investigated the dynamical stability of the five lowest energy structures (A, B, C, D, and E) through *Ab Initio* Molecular Dynamics (AIMD) simulations, using the SIESTA code. This is a procedure that has been previously used to predict the thermal stability of materials.[70,71] In our calculations, we evolved each structure in the NPT ensemble for 2 ps, with a time step of 1 fs. Temperature and in-plane pressure components were controlled using a Nosé–Hoover thermostat and a Parrinello–Rahman barostat. In Fig. 3(a), we present snapshots of the structures after completion of the AIMD simulations at 300 K. Careful inspection of the snapshots reveals that the thermal motion caused slight structural deformation. More importantly, inspection also reveals that the underlying atomic lattice remained intact, as no bonds were broken during the dynamics. Furthermore, we also carried out calculations at higher temperatures for structure A. Our results, presented in Fig. 3(b),

indicate that this particular structure should remain stable even at temperatures as high as 2000 K.

Let us now discuss the electronic properties of the eleven $B_xC_yN_z$ hybrid α-graphynes investigated in this work. We performed the calculations using the PBE and HSE06 exchange-correlation functionals using the SIESTA and GAUSSIAN16 packages, respectively. The energy gap values E_g are shown in the sixth and seventh columns of Table 1 – we found E_g values ranging from 0.0 to 1.43 eV for the PBE approach and 0.02 to 2.00 eV for the HSE06 one. We notice that, in general, our results are as expected, since the PBE approach underestimates E_g values. Only for structure L, we obtained a higher value with the PBE approach. However, in this particular case, the difference between the gap values is so small (0.05 eV) that we can consider both approaches predict the same electronic behavior. At the same time, we verified that, in the PBE approach, only structures G and H are metallic. All the other structures behave as semiconductors, in both approaches, irrespective of the atomic arrangement in the unit cell. This behavior is due to the electronic configuration of the lattice, with a mixture of sp^2 and sp orbitals. In Fig. 4 we present their calculated electronic band structure, with 100 k-points along the Γ–X–Z direction. Moreover, it is important to note that the energy gap values determined for the $B_xC_yN_z$ hybrid α-graphynes are intermediate to those found in α-graphyne and α-BNyne.[51]
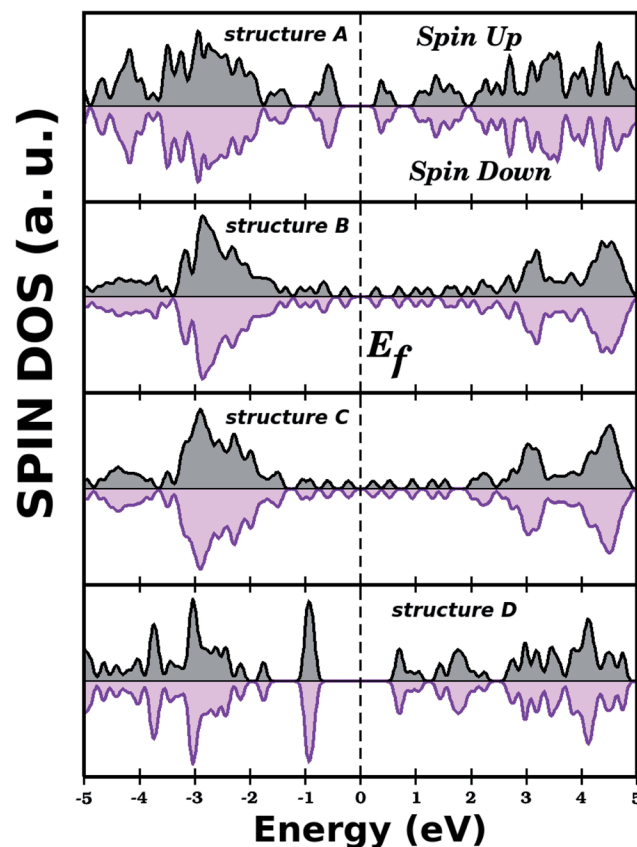

Fig. 6 Densities of states (spin up and down) for selected $B_xC_yN_z$ hybrid α-graphynes. The total spin is zero for all investigated structures.

Regarding the electronic states near the Fermi energy (E_f), projected density of states (PDOS) calculations reveal that, in general, carbon atoms are the major contributors to these states, see Fig. 5. Complementary local density of states (LDOS) calculations are also displayed in Fig. 5, and they reveal that the bottom of the conduction band and the top of the valence band are associated with p_z orbitals of C atoms, in full agreement with PDOS results. Finally, no relationship was observed between energy gap values and R_b/W_b bond ratios, which indicates that the energy gap of a $B_xC_yN_z$ hybrid α-graphyne depends strongly on the particulars of its atomic arrangement. As a side note, in Fig. 6 we show the calculated spin polarization for selected structures. Calculations reveal a spin value of zero for all $B_xC_yN_z$ hybrid α-graphynes; this means their valence bands are completely filled, without unpaired electrons.

In order to analyze the optical properties of the $B_xC_yN_z$ hybrid α-graphynes we have calculated the optical absorption spectrum as function of the photon energy. The analysis of this spectrum is an important starting point for predicting if the investigated structures are promising for future applications in optoelectronic devices. Firstly, the frequency-dependence of the complex dielectric function $\varepsilon(\omega) = \varepsilon_1(\omega) - i\varepsilon_2(\omega)$ is calculated. The imaginary part is directly proportional to the optical absorption spectrum, which is calculated from the time dependent perturbation theory in the simple dipole approximation, which is given by
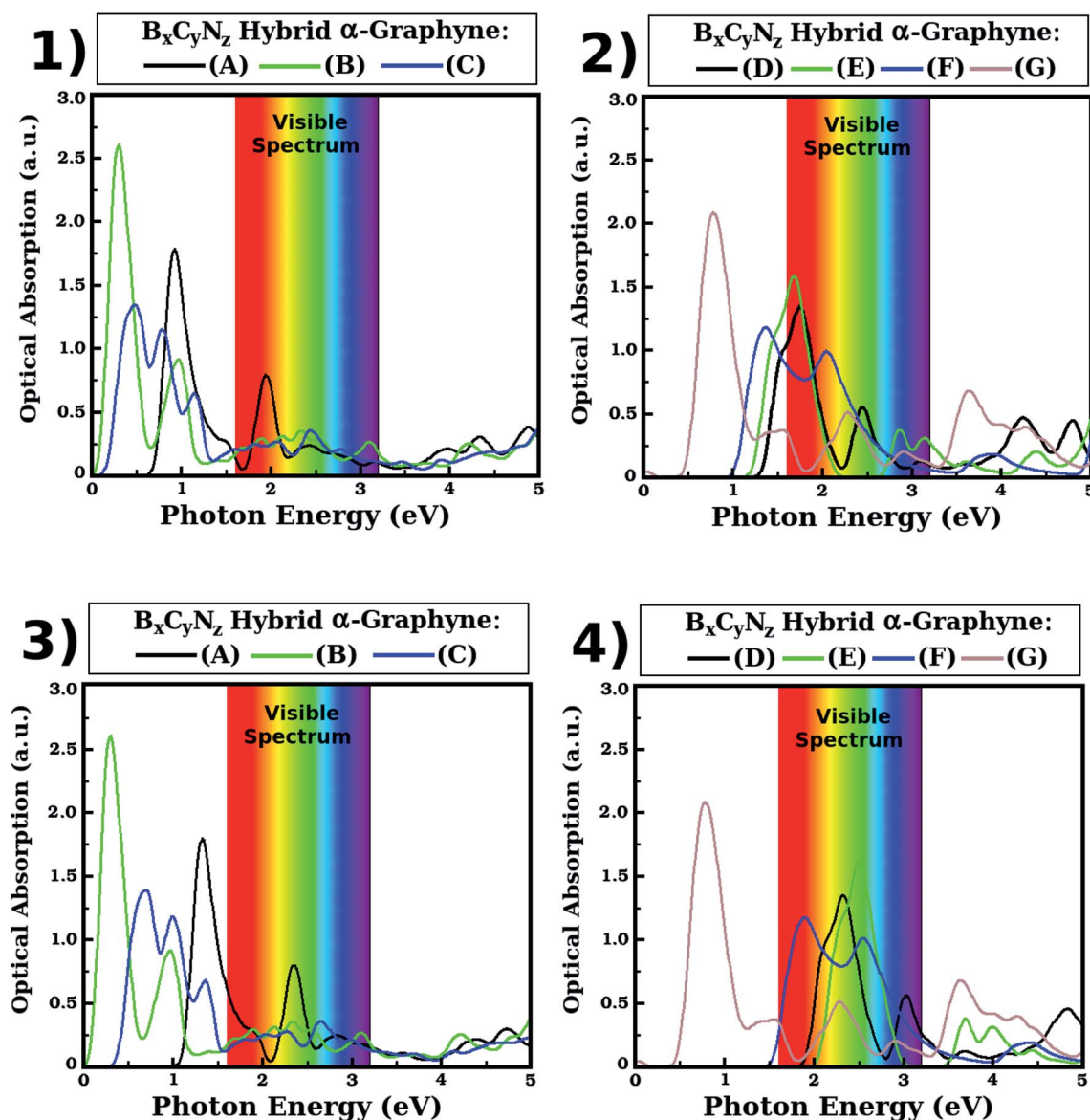

Fig. 7 Optical absorption spectrum as function of the photon energy for selected $B_xC_yN_z$ hybrid α-graphynes, with the light polarization perpendicular to the α-graphynes's plane. At (1) and (2), the absorption spectrum was obtained from calculations with the PBE functional. At (3) and (4), the absorption spectrum was corrected using the scissor operator available in the SIESTA code. This correction method uses the difference between the energy gap values obtained with the HSE06 and PBE functionals.

$$\varepsilon_2(\omega) = \frac{8\pi^2 e^2}{m^2 \omega^2 \Omega} \sum_{cv} \sum_{k} |\langle \psi_{ck}|\hat{\mathbf{e}} \cdot \mathbf{p}|\psi_{vk}\rangle|^2 \times \delta(E_{ck} - E_{vk} - \hbar\omega), \quad (4)$$

for a vertical transition from a filled valence band $\langle \psi_{vk}|$ of energy E_{vk} to an empty conduction band $|\psi_{ck}\rangle$ of energy E_{ck} with the same wave vector $\mathbf{k}$. The parameter ω is the angular frequency of the incident radiation, Ω represents the volume of the supercell, m is the electron mass, $\mathbf{p}$ is the momentum operator, and $\hat{\mathbf{e}}$ is the unit vector of polarization in the direction of the incident electric field. The results obtained with the PBE functional are presented in Fig. 7(a). Moreover, we employed the scissor operator available in the SIESTA code in order to correct the optical spectrum obtained with the PBE functional (see Fig. 7(b)). In this correction, the value of the scissor operator is given by the difference between the energy gap values obtained with the HSE06 and PBE approaches. Recent works have employed this methodology to accurately predict the optical

properties of nanomaterials.[72–74] Thus, as illustrated in Fig. 7, after the introduction of this correction., we observed a shift in the optical spectra of structures A, C, D, E and F. For structures B and G, the value of the scissor operator was very small, and the optical spectrum did not present appreciable changes.

We found that the optical absorption of the $B_x C_y N_z$ hybrid α-graphynes is in the infrared region for the three lowest energy structures (A, B and C) and for structure G, while for some of the other structures absorption occurs in the visible region. Indeed, as can be seen in Fig. 7, for structures A, B, C and G the first absorption peak occurs in the infrared at about 1.34, 0.30, 0.70 and 0.78 eV. For structures D, E and F, the first absorption peak occurs in the visible region at about 2.32 (green), 2.51 (green) and 1.90 (red) eV. These peaks correspond to a first optical transition between the top of the valence band and the bottom of the conduction band in carbon atoms, as we can see in the
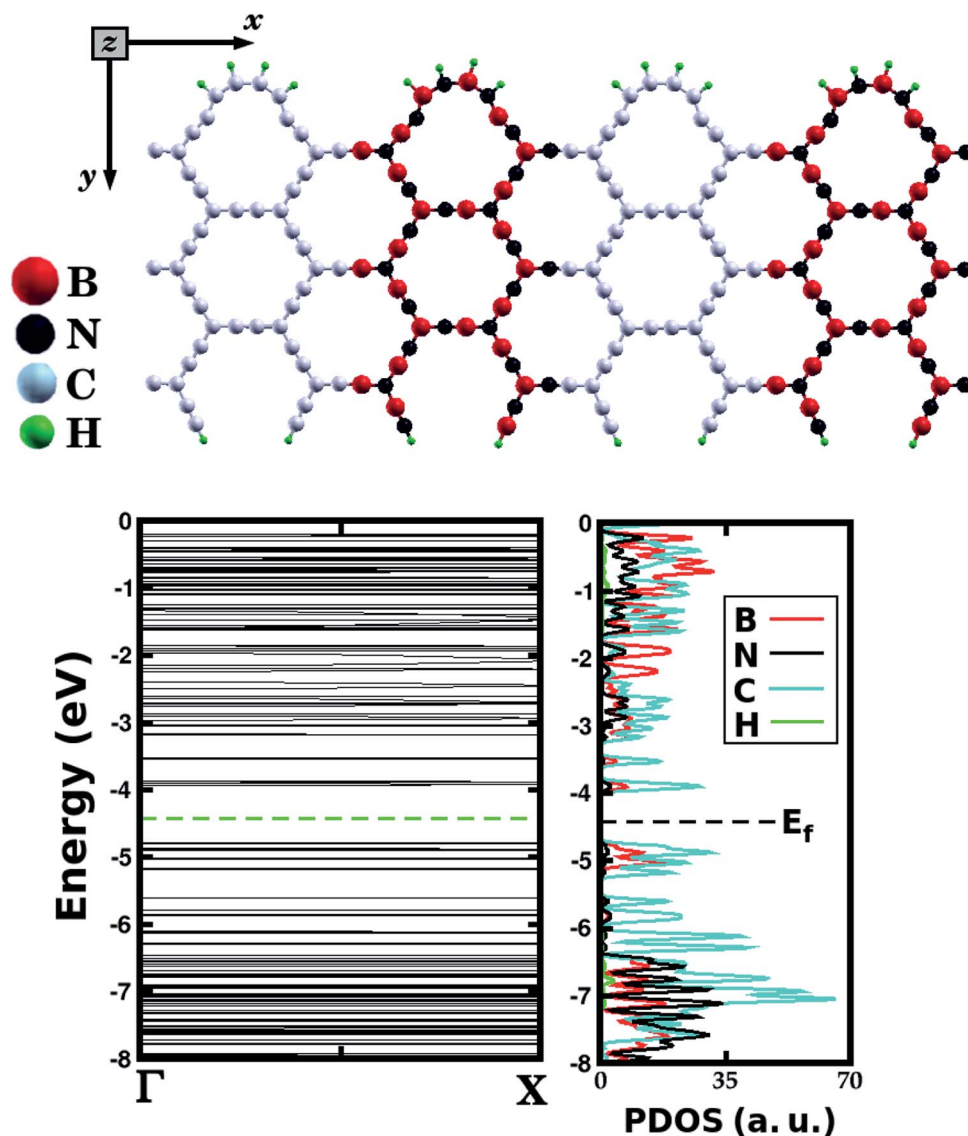

Fig. 8 Optimized B–C–N hybrid α-graphyne nanoribbon with armchair edge. The calculated band structure and the projected density of states (PDOS) are also shown. The Fermi energy E_f is indicated by the horizontal dotted line.

projected density of states (Fig. 5). Given that the maximum optical absorption occurs in the infrared for the three lowest energy hybrid α-graphynes, we note that these materials are likely good candidates for use in nanoscale optical devices that operate in this region of the electromagnetic spectrum, such as heat sensors. They could also be potentially used in infrared radiation filters, which are typically used to absorb heat.

Regarding the other absorption peaks, we note that some structures still present peaks in the infrared region. Specifically, the second peak for structure B is found approximately at 0.98 eV, while the second and third peaks for structure C occur approximately at 1.00 and 1.36 eV. Meanwhile, the second absorption peak for structures A, D and F occurs in the visible region, at about 2.36 (green), 3.04 (violet) and 2.54 (green) eV. For structures E and G, the second absorption peak is in the ultraviolet region (at about 3.70 and 3.64 eV, respectively). Additionally, with the exception of structure C, we found that the third absorption peak occurs either in the visible (green) or in the ultraviolet region.

Additionally, we carried out first-principles calculations to investigate the electronic properties of a particular B–C–N hybrid α-graphyne nanoribbon, which is illustrated in Fig. 8. Such structure was constructed based on the atomic arrangement of monolayer A (see Fig. 1), which corresponds to the most stable structure among all investigated $B_xC_yN_z$ hybrid α-graphynes. The proposed nanoribbon is composed of BN and C stripes, which are perpendicular to the periodic direction, with armchair symmetry. Hydrogen atoms were also included at the nanoribbon edges. After the optimization process, notice that C–C and B–N bonds undergo deformation, modifying the shape of the local hexagons. Band structure calculations reveal that this nanoribbon is a semiconductor material, with an energy gap of 0.83 eV, which is very close to that of monolayer A (a difference of 0.03 eV). Finally, observe in the PDOS results (also displayed in Fig. 8) that electronic states near the Fermi level are associated with carbon and boron atoms.

IV. Conclusions

In summary, we employed DFT calculations to investigate the stability, as well as the electronic and optical properties, of eleven two-dimensional structures composed of boron, nitrogen, and carbon. In the proposed monolayers, atoms were positioned following an α-graphyne pattern, and hence were termed $B_xC_yN_z$ hybrid graphynes. Unlike previous investigations into such hybrid materials, we also considered island- and stripe-like atomic arrangements of B, C, and N. Overall, we found that the stability of the proposed structures increased when the number of carbon-boron and carbon-nitrogen bonds decreased and, consequently, that island- and stripe-like arrangements were more stable than mixed arrangements of B, C, and N. On the other hand, in our calculations we found no relationship between the number of carbon–boron and carbon–nitrogen bonds and the electronic properties. We determined that $B_xC_yN_z$ hybrid α-graphynes are semiconducting, with band gap values ranging from 0.02 to 2.00 eV. We also performed PDOS and LDOS calculations, to investigate the electronic states

near the Fermi level (E_f). Our results reveal that both states at the top of the valence band and at the bottom of the conduction band are associated with carbon atoms. Finally, we determined the optical absorption spectra of the proposed structures. We found that eight of the proposed monolayers present absorption peaks in various regions of the infrared, with the remaining three presenting absorption peaks in the visible spectrum. Our calculations indicate that the $B_xC_yN_z$ hybrid α-graphynes are viable candidates for optoelectronic devices that operate in the infrared region of the electromagnetic spectrum, such as heat sensors and infrared filters.

Conflicts of interest

There are no conflicts to declare.

Acknowledgements

References

1 A. H. C. Neto, F. Guinea, N. M. R. Peres, K. S. Novoselov and A. K. Geim, *Rev. Mod. Phys.*, 2009, **81**, 109–162.
2 A. K. Geim, *Science*, 2009, **324**, 1530–1534.
3 D. Pacile, J. C. Meyer, C. O. Girit and A. Zettl, *Appl. Phys. Lett.*, 2008, **92**, 133107.
4 C. H. Jin, F. Lin, K. Suenaga and S. Iijima, *Phys. Rev. Lett.*, 2009, **102**, 195505.
5 S. D. Sarma, A. Shaffique, E. H. Hwang and R. Enrico, *Rev. Mod. Phys.*, 2011, **83**, 407–470.
6 E. Gibney, *Nature*, 2015, **522**, 274.
7 C. Lee, X. Wei, J. W. Kysar and J. Hone, *Science*, 2008, **321**, 385–388.
8 X. Ma and H. Zhang, *Nanoscale Res. Lett.*, 2013, **8**, 440.
9 W. Han, L. Wu, Y. Zhu, K. Watanabe and T. Taniguchi, *Appl. Phys. Lett.*, 2008, **93**, 223103.
10 Y. Miyamoto, M. L. Cohen and S. G. Louie, *Phys. Rev. B: Condens. Matter Mater. Phys.*, 1995, **52**, 14971–14975.
11 S. Azevedo, J. Kaschny, M. Caio and F. de Brito Mota, *Eur. Phys. J. B*, 2009, **67**, 507–512.
12 S. Azevedo and R. De Paiva, *Europhys. Lett.*, 2006, **75**, 126–132.
13 S. Azevedo, M. Mazzoni, R. Nunes and H. Chacham, *Phys. Rev. B: Condens. Matter Mater. Phys.*, 2004, **70**, 205412.
14 S. Azevedo, J. R. Kaschny, C. Castilho and F. B. Mota, *Nanotechnology*, 2007, **18**, 495707.
15 L. Ci, L. Song, C. Jin, D. Jariwala, D. Wu, Y. Li, A. Srivastava, Z. F. Wang, K. Storr, L. Balicas, F. Liu and P. M. Ajayan, *Nat. Mater.*, 2010, **9**, 430–435.
16 C. Huang, C. Chen, M. Zhang, L. Lin, X. Ye, S. Lin, M. Antonietti and X. Wang, *Nat. Commun.*, 2015, **6**, 7698.

17 M. S. Mazzoni, R. W. Nunes, S. Azevedo and H. Chacham, *Phys. Rev. B: Condens. Matter Mater. Phys.*, 2006, **73**, 073108.

18 Y. Tateyama, T. Ogitsu, K. Kusakabe, S. Tsuneyuki and S. Itoh, *Phys. Rev. B: Condens. Matter Mater. Phys.*, 1997, **55**, R10161–R10164.

19 A. K. Manna and S. K. Pati, *J. Phys. Chem. C*, 2011, **115**, 10842–10850.

20 A. Freitas, S. Azevedo, M. Machado and J. R. Kaschny, *Appl. Phys. A*, 2012, **108**, 185–193.

21 A. Du, Z. Zhu, G. Lu and S. C. Smith, *J. Am. Chem. Soc.*, 2009, **131**, 1682–1683.

22 M. Becton, L. Zhang and X. Wang, *Phys. Chem. Chem. Phys.*, 2014, **16**, 18233.

23 W. S. Cranford, B. D. Brommer and J. M. Buehler, *Nanoscale*, 2012, **4**, 7797–7809.

24 A. Freitas, L. D. Machado, C. G. Bezerra, R. M. Tromer, L. F. C. Pereira and S. Azevedo, *RSC Adv.*, 2018, **8**, 24847.

25 Z. Wang, X. Zhou, X. Zhang, Q. Zhu, H. Dong, M. Zhao and A. R. Oganov, *Nano Lett.*, 2015, **15**, 6182–6186.

26 Y. Liu, G. Wang, Q. Huang, L. Guo and X. Chen, *Phys. Rev. Lett.*, 2012, **108**, 225505.

27 G. R. Bhimanapati, Z. Lin, V. Meunier, Y. Jung, J. Cha, S. Das, D. Xiao, Y. Son, M. S. Strano, V. R. Cooper, L. Liang, S. G. Louie, E. Ringe, W. Zhou, S. S. Kim, R. R. Naik, B. G. Sumpter, H. Terrones, F. Xia, Y. Wang, J. Zhu, D. Akinwande, N. Alem, J. A. Schuller, R. E. Schaak, M. Terrones and J. A. Robinson, *ACS Nano*, 2015, **9**, 11509–11539.

28 R. H. Baughman, H. Eckhardt and M. J. Kertesz, *J. Chem. Phys.*, 1987, **87**, 6687–6698.

29 D. Sundholm, L. N. Wirz and P. Schwerdtfeger, *Nanoscale*, 2015, **7**, 15886–15894.

30 J. M. Kehoe, J. H. Kiley, J. J. English, C. A. Johnson, R. C. Petersen and M. M. Haley, *Org. Lett.*, 2000, **2**, 969–972.

31 F. Diederich, *Nature*, 1994, **369**, 199–207.

32 M. M. Haley, S. C. Brand and J. J. Pak, *Angew. Chem., Int. Ed.*, 1997, **36**, 836–838.

33 K. Tahara, Y. Yamamoto, D. E. Gross, H. Kozuma, Y. Arikuma, K. Ohta, Y. Koizumi, Y. Gao, Y. Shimizu, S. Seki, K. Kamada, J. S. Moore and Y. Tobe, *Chem.–Eur. J.*, 2013, **19**, 11251–11260.

34 G. Li, Y. Li, H. Liu, Y. Guo, Y. Li and D. Zhu, *Chem. Commun.*, 2010, **46**, 3256–3258.

35 W. Z. Wu, W. L. Guo and X. C. Zeng, *Nanoscale*, 2013, **5**, 9264–9276.

36 D. Malko, C. Neiss, F. Vines and A. Gorling, *Phys. Rev. Lett.*, 2012, **108**, 086804.

37 V. R. Coluci, S. F. Braga, S. B. Legoas, D. S. Galvao and R. H. Baughman, *Phys. Rev. B: Condens. Matter Mater. Phys.*, 2003, **68**, 035430.

38 H. J. Hwang, Y. Kwon and H. Lee, *J. Phys. Chem. C*, 2012, **116**, 20220–20224.

39 H. J. Hwang, J. Koo, M. Park, N. Park, Y. Kwon and H. Lee, *J. Phys. Chem. C*, 2013, **117**, 6919–6923.

40 H. Y. Zhang, X. J. He, M. W. Zhao, M. Zhang, L. X. Zhao, X. J. Feng and Y. H. Luo, *J. Phys. Chem. C*, 2012, **116**, 16634–16638.

41 J. Kou, X. Zhou, H. Lu, F. Wu and J. Fan, *Nanoscale*, 2014, **6**, 1865–1870.

42 N. Narita, S. Nagai, S. Suzuki and K. Nakao, *Phys. Rev. B: Condens. Matter Mater. Phys.*, 1998, **58**, 11009–11014.

43 J. Zhou, K. Lv, Q. Wang, X. S. Chen, Q. Sun and P. J. Jena, *Chem. Phys.*, 2011, **134**, 174701.

44 L. D. Pan, L. Z. Zhang, B. Q. Song, S. X. Du and H. J. Gao, *Appl. Phys. Lett.*, 2011, **98**, 173102.

45 Y. Zhang, J. Yun, K. Wang, X. Chen, Z. Yang, Z. Zhang, J. Yan and W. Zhao, *Comput. Mater. Sci.*, 2017, **136**, 12–19.

46 X. Cao, Y. Li, X. Cheng and Y. Zhang, *Chem. Phys. Lett.*, 2011, **502**, 217–221.

47 S. Behzad, *Phys. E*, 2016, **83**, 211–214.

48 J. Yun, Y. Zhang, K. Wang and Z. Zhang, *Comput. Mater. Sci.*, 2016, **123**, 79–84.

49 A. N. Enyashina, A. A. Sofronova, Y. N. Makurina and A. L. Ivanovskii, *J. Mol. Struct.*, 2004, **684**, 29–33.

50 C. Sun, Y. Liu, J. Xu, B. Chi, C. Bai, S. Li, X. Zhao and X. Li, *Phys. E*, 2015, **70**, 190–197.

51 V. O. Ongun and S. Ciraci, *J. Phys. Chem. C*, 2013, **117**, 2175–2182.

52 J. Yun, Y. Zhang, M. Xu, J. Yan, W. Zhao and Z. Zhang, *J. Mater. Sci.*, 2017, **52**, 10294–10307.

53 X. Deng, M. Si and J. Dai, *J. Chem. Phys.*, 2012, **137**, 201101.

54 D. Sánchez-Portal, P. Ordejón, E. Artacho and J. M. Soler, *Int. J. Quantum Chem.*, 1997, **65**, 453–461.

55 J. M. Soler, E. Artacho, J. D. Gale, A. García, J. Junquera, P. Ordejón and D. Sánchez-Portal, *J. Phys.: Condens. Matter*, 2002, **14**, 2745.

56 W. Kohn and L. J. Sham, *Phys. Rev. Lett.*, 1965, **140**, A1133–A1138.

57 J. P. Perdew, K. Burke and M. Ernzerhof, *Phys. Rev. Lett.*, 1996, **77**, 3865–3868.

58 N. Troullier and J. L. Martins, *Phys. Rev. B: Condens. Matter Mater. Phys.*, 1991, **43**, 1993–2006.

59 L. Kleinman and D. M. Bylander, *Phys. Rev. Lett.*, 1982, **48**, 1425–1428.

60 M. A. Marques, J. Vidal, M. J. Oliveira, L. Reining and S. Botti, *Phys. Rev. B: Condens. Matter Mater. Phys.*, 2011, **83**, 035119.

61 T. O. Wehling, E. Sasioglu, C. Friedrich, A. I. Lichtenstein, M. I. Katsnelson and S. Blugel, *Phys. Rev. Lett.*, 2011, **106**, 236805.

62 S. Lee, S. Kim and K. Kim, *Phys. Rev. B: Condens. Matter Mater. Phys.*, 2012, **86**, 155436.

63 B. Dong, H. Guo, Z. Liu, T. Yang, P. Tao, S. Tang, R. Saito and Z. Zhanga, *Carbon*, 2018, **131**, 223.

64 I. Alcon, F. Vines, I. de P. R. Moreira and S. T. Bromley, *Nat. Commun.*, 2017, **8**, 1957.

65 J. Heyd and G. E. Scuseria, *J. Chem. Phys.*, 2004, **121**, 1187.

66 P. Deak, B. Aradi, T. Frauenheim, E. Janzen and A. Gali, *Phys. Rev. B: Condens. Matter Mater. Phys.*, 2010, **81**, 153203.

67 M. J. Frisch, *et al.*, *Gaussian 16, Revision C.01*, Gaussian, Inc., Wallingford CT, 2016.

68 A. V. Krukau, O. A. Vydrov, A. F. Izmaylov and G. E. Scuseria, *J. Chem. Phys.*, 2006, **125**, 224106.

69 A. C. M. Carvalho, C. G. Bezerra, J. A. Lawlor and M. S. Ferreira, *J. Phys.: Condens. Matter*, 2014, **26**, 015303.

70 G. Zhu, Q. Sun, Y. Kawazoe and P. Jena, *Int. J. Hydrogen Energy*, 2015, **40**, 3689.

71 E. Montes and U. Schwingenschlogl, *Phys. Rev. B*, 2016, **94**, 035412.

72 P. Nayebi, M. Emami-Razavi and E. Zaminpayma, *J. Phys. Chem. C*, 2016, **120**, 4589.

73 M. P. Ljungberg, O. Vanska, P. Koval, S. W. Koch, M. Kira and D. Sanchez-Portal, *New J. Phys.*, 2017, **19**, 033019.

74 M. Kolos and F. Karlicky, *Phys. Chem. Chem. Phys.*, 2019, **21**, 3999.